Nano Research
2023, 16(12): 13381–13391

ISSN 1998-0124 CN 11-5974/O4
https://doi.org/10.1007/s12274-023-5948-8

Research Article

Dual-responsive fiber-reinforced hydrogel actuators by direct ion patterning

Mingyuan Zhao[1,2,§], Dong Han[1,2,§], Yuan Meng[1,2], Jing Liu[1], Yuting Zhu[1], Zhongxian Li[1,2], Kai Li[3], Wentao Liu[1] (✉), and Zhuo Ao[1] (✉)

[1] CAS Center for Excellence in Nanoscience, National Center for Nanoscience and Technology, Beijing 100190, China
[2] School of Future Technology, University of Chinese Academy of Sciences, Beijing 100049, China
[3] College of Life Sciences, Beijing University of Chinese Medicine, Beijing 100029, China
[§] Mingyuan Zhao and Dong Han contributed equally to this work.

© Tsinghua University Press 2023

Received: 29 April 2023 / **Revised:** 14 June 2023 / **Accepted:** 21 June 2023

ABSTRACT

Nature inspired deformable heterogeneous smart hydrogels have attracted much attention in many fields such as biomedicine devices and soft actuators. However, normal spatial heterogeneous hydrogel structures can only respond to single factor and take one action as set in fabrication. Herein, we report a pre-stretched metal-liganded shape memory hydrogel with fiber reinforced, P(AAc-co-AAm)/CCNFs-Fe^{3+} (CCNFs: carboxylated cellulose nanofibers, AAc: acrylic acid, AAm: acrylamide), which can conduct shape deformation by solvent induction and ultraviolet (UV) light. The deformation pattern could be programmed by the deposing of ferroin ions. Also, the pre-stretched shape memory hydrogels could effectively produce cyclic actuation or complex shape actuation by UV light. More importantly, combining the solvent response with the light response enabled complex reversible actuations, such as simulating the bending and unfolding of fingers. The addition of CCNFs significantly enhanced the mechanical properties of the hydrogels. The hydrogels with 3 wt.% CCNFs showed an elongation at break of about 500% and a significant increase in tensile strength of 8.7-fold to 1.55 MPa after coordination with metal ions, which was able to meet the mechanical requirements of the bionic actuated hydrogels. This work demonstrated that combining light-programmed and light-responsive shape-memory hydrogels, complemented by another independent response property, could achieve complex and reversible programmed actuations.

KEYWORDS

dual responsive hydrogel, shape deformation, metal ion pattern, carboxylated cellulose nanofibers (CCNFs), light induction

1 Introduction

In living organisms, shape deformation systems often present in heterogeneous microstructures. For example, the opening and closing of pine cones and the helical behavior of zinnia pods depend on the orientation of the cellulose microfibrils. The tissue exhibits anisotropic expansion or contraction in the direction perpendicular to the original fibers while water is absorbed or expelled [1, 2]. Bird feathers have been found to recover their innate shape and mechanical strength through hydration [3, 4]. These potential deformation mechanisms have inspired the development of novel responsive biomimetic materials. To date, a more desirable candidate that can mimic the deformation or shape transformation behavior of living organisms is a hydrogel that resembles biological tissues and has multiple responsive properties. Smart hydrogels respond to different forms of stimuli such as temperature [5], humidity [6, 7], light [8–11], electricity [12], and magnetic fields [13] by changing their volume [14], color [15, 16], and other properties. In fact, the key aspect of constructing smart hydrogels is to construct spatially heterogeneous structures. Many researches have been devoted to the preparation of hydrogels with inhomogeneous structures, such as bilayer hydrogels [17–19], photomask templates [20, 21], gradient chemical synthesis [22, 23], or oriented fillers [12, 24]. The anisotropic structure of such hydrogel drivers is given upon chemical programming. The deformation behavior of the drivers cannot be readjusted as needed, and the feedstock is generally not recyclable or reprogrammable. Therefore, it is urgent to develop a hydrogel with superior mechanical properties that is reprogrammable and can achieve more complex and controllable shape deformation.

Applying uneven stimuli to the surface of homogeneous hydrogels is the key to achieving complex and controllable deformations. The addition of metal ions as heterogeneous elements into homogeneous hydrogels by patterning for programmable deformation has been extensively studied [25, 26]. The mechanical properties of the hydrogels are enhanced by the chemical introduction of metal ions, and the resulting metal-ligand structure provides a reversible molecular switch for the hydrogels to memorize a specific shape and respond to stimuli. The ligand interaction can be reduced or eliminated to ensure the reprogrammability of the gel under the corresponding solvent or

Address correspondence to Wentao Liu, liuwentao@nanoctr.cn; Zhuo Ao, aoz@nanoctr.cn

light stimuli. However, hydrogels programmed with metal ions alone are difficult to achieve better fixation and recovery of elastic deformation and are unable to store and release high elastic energy during deformation [27, 28]. It is well known that pre-stretching techniques usually exhibit strong and extremely rapid deformation due to their deformation being mainly driven by rapid shrinkage stresses and asymmetric release rather than asymmetric swelling [29–31]. To overcome the above problems, pre-stretching techniques can be introduced into metal-ligand hydrogel systems to form pre-stresses for robust deformation response.

However, the shape memory effect brought by metal-ligand hydrogels usually only enables simple shape deformation through reversible non-covalent interactions and still requires reprogramming by external loading at different deformation cycles. For this reason, many studies have sought to combine shape memory polymers with multiple stimulus forms to achieve the integration of shape memory functions and self-deformation behavior [32–35]. Light, as a non-contact, high spatio-temporal resolution, and good tissue penetration form of stimulation, can satisfy the need for local stimulation or progressive deformation [36]. However, previous studies have shown that the combination of shape memory properties and optical response basically only achieves shape recovery [37, 38]. Once the shape is recovered, it is difficult to control its response again by light for the next cycle. Therefore, adding another response mechanism (e.g., solvent) to the system is expected to achieve more complex and reversible programmed deformation and significantly improve the programmability and reversibility of the hydrogels.

In this work, we report a simple strategy of selecting carboxylated cellulose nanofibers (CCNFs) reinforced P(AAc-co-AAm)/CCNFs (AAc: acrylic acid, AAm: acrylamide) hydrogels to prepare programmable and multi-responsive supramolecular shape memory hydrogels by pre-stretching and chelating with trivalent iron ions (Fe^{3+}). The addition of CCNFs significantly enhanced the mechanical properties of the hydrogels and optimized their shape memory performance. The deformation effect of the hydrogels could be precisely controlled by adjusting the experimental conditions such as the ratio of CCNFs, concentration of Fe^{3+}, percentage of pre-stretching, thickness of the hydrogels, and light irradiation time. The reprogrammability of the hydrogels was also confirmed. In particular, metal ions programmed hydrogels were shown to deform due to differential swelling in water or ethanol. Asymmetric release of stress leads to bending or shrinking of ultraviolet (UV) light programmable induced pre-stretched shape memory hydrogels. Importantly, the programmed deformation designed according to the process "supramolecular shape memory–local light reduction–solvent reversible driving" is presented in a simulated finger actuation process. The application of this simple hydrogel system offered the possibility of shape memory hydrogel actuation behavior and development of bionic systems.

2 Experimental

2.1 Materials

AAc (> 99%), CCNFs (diameter: 50 nm, length: 1–3 μm), and N,N'-methylenebisacrylamide (NMBA, 99%) were purchased from Shanghai Maclean Biochemical Technology Co. AAm (99.0%) and potassium persulfate (KPS, 99.99%) were purchased from Shanghai Aladdin Biochemical Technology Co. Ferric chloride hexahydrate ($FeCl_3{\cdot}6H_2O$, 98.5%), lactic acid (DL-Lactic acid), hydrochloric acid (HCl), and sodium hydroxide (NaOH) were purchased from China National Pharmaceutical Group Chemical Reagent Co. Deionized water was used in all the experiments unless otherwise specified. The acrylic acid was pretreated by reduced-pressure distillation to remove inhibitors, and the other reagents were used without further purification.

2.2 Synthesis of P(AAc-co-AAm)/CCNFs hydrogels

The formulation of P(AAc-co-AAm) hydrogels prepared by other researchers was referred and the addition ratio of CCNFs was explored [30]. Briefly, AAm (20 wt.%, weight ratio of AAm/H_2O) and AAc (5 wt.%, weight ratio of AAc/H_2O) were dissolved in an appropriate amount of deionized water and sonicated until complete dissolution. The corresponding masses of CCNFs (0 wt.%, 1 wt.%, 2 wt.%, and 3 wt.%, weight ratio of CCNFs/H_2O) were weighed and placed in the above solution and stirred at room temperature for 3 h. Subsequently, NMBA (0.04 wt.%, weight ratio of NMBA/H_2O) and KPS (0.1 wt.%, weight ratio of KPS/H_2O) were added separately and stirred rapidly. The obtained prepolymerization solution was poured into a mold consisting of two glass plates and a silicone gasket. The template was removed after polymerization at 60 °C for 10 h to obtain homogeneous P(AAc-co-AAm)/CCNFs hydrogels.

2.3 Preparation of pre-stretched P(AAc-co-AAm)/CCNFs-Fe^{3+} hydrogels

The ends of P(AAc-co-AAm)/CCNFs hydrogels were fixed with three-dimensional (3D) printed jigs and stretched to a preset length. The P(AAc-co-AAm)/CCNFs-Fe^{3+} hydrogels were obtained by soaking in ferric chloride solution and then washing with deionized water and wiping dry.

2.4 Characterization

2.4.1 Microstructure

The samples to be tested were prepared and sprayed with gold, and the microstructure of the hydrogels was observed using the cold field emission scanning electron microscopy (SEM) (S-4800, Hitachi, Japan) at an accelerating voltage of 10.0 kV. X-ray energy spectrum analysis of the microscope was used to characterize the distribution of C, N, O, and Fe elements in the longitudinal section of the hydrogels. The samples used for SEM and energy dispersive X-ray spectroscopy (EDS) were swollen and freeze-dried.

2.4.2 Fourier transform infrared (FTIR) spectroscopy analysis

The samples were analyzed by FTIR spectroscopy using the microscopic infrared spectrometer (SP-200i, Perkin Elmer, USA) in the wavelength range of 4000–400 cm^{-1}. Potassium bromide powder compacts were used as background with 32 scans. The samples used for FTIR were swollen and freeze-dried.

2.4.3 Diffuse reflectance UV–visible (UV–Vis) spectroscopy

Diffuse reflectance UV–Vis spectra of hydrogel samples at different ethylenediamine tetraacetic acid (EDTA) chelation time from 300 to 600 nm were recorded using the UV integrating sphere attachment of the UV–Vis NIR spectrophotometer (Lambda 1050+, Perkin Elmer, USA).

2.4.4 Mechanical property measurement

Tensile tests were performed in the universal tensile testing machine (Suns UTM2103, Shenzhen, China). A 50 N load cell was selected for the experiment. Measurements were performed on P(AAc-co-AAm)/CCNFs and P(AAc-co-AAm)/CCNFs-Fe^{3+} rod hydrogels with different CCNFs contents. The Fe^{3+} concentration used was 0.1 M. Both ends of the hydrogel were fixed to the fixture of the tensile tester for stress–strain testing until the

hydrogel was pulled off and stopped running. The tensile speed was 8 mm/min and three parallel experiments were performed in each group.

2.4.5 Swelling behavior

Consistently sized P(AAc-co-AAm)/CCNFs, P(AAc-co-AAm)/CCNFs-Fe^{3+}, and light-reduced P(AAc-co-AAm)/CCNFs-Fe^{2+} hydrogels were freeze-dried and then swollen in deionized water. The hydrogels were dried and weighed at 0, 2, 4, 6, 12, 24, and 48 h. The initial mass of the hydrogels after freeze-drying is recorded as M_0. The mass after t h of swelling is M_t. The swelling rate is recorded as SR, and the equation of swelling rate is

$$\mathrm{SR}\ (\%) = \frac{M_t - M_0}{M_0} \times 100\% \quad (1)$$

2.5 Evaluation of shape memory properties

Pre-stretch lengths were set for the original hydrogels according to different pre-stretch percentages. The initial pre-stretch length is L_0. The length obtained after fixation and release is L_1. The shape fixation rate is called SFR, and then the shape fixation rate equation is

$$\mathrm{SFR}\ (\%) = \frac{L_1}{L_0} \times 100\% \quad (2)$$

2.6 Metal ion programming causing swelling deformation

The hydrogels were individually cut into corresponding shapes and patterned with 0.1 M $FeCl_3$ solution for coating. After a certain time, the residual $FeCl_3$ solution on the surface was washed off to prevent further chelation. The hydrogels were soaked and swollen in deionized water.

2.7 Water-ethanol swelling cycle

The hydrogels were cut into strips of specific size. The $FeCl_3$ solution was applied to one side of the hydrogel and kept for 3 min before removing the surface residue. The hydrogels were dissolved in water for 4 min and transferred to anhydrous ethanol for 3 min. The hydrogels were soaked in water and anhydrous ethanol solution for 5 cycles alternately and photographed for recording. The angles were measured with a full-circle meter.

2.8 Light fixed-point programming to induce hydrogel deformation

The hydrogels were cut into specific shapes. The hydrogels were stretched by 300% using a 3D printed stretching jig. The hydrogels were immersed in 0.1 M $FeCl_3$ solution for a certain time and then washed with deionized water followed by wiping dry. The hydrogels were soaked in sodium lactate solution and then irradiated with UV light to make the hydrogels bend and deform.

3 Results and discussion

3.1 Preparation and characterization of P(AAc-co-AAm)/CCNFs-Fe^{3+} hydrogels

Pre-stretched fiber-reinforced metal-liganded P(AAc-co-AAm)/CCNFs-Fe^{3+} hydrogels (abbreviated as SMCH) were prepared by the scheme shown in Fig. 1. First, a mixture of acrylamide and acrylic acid was co-polymerized into the first covalent cross-linked network P(AAc-co-AAm)/CCNFs in the presence of CCNFs. CCNFs were involved in additional cross-linking of non-covalent bonds, such as coordination bonds and hydrogen bonds. Next, the pre-stretched P(AAc-co-AAm)/CCNFs hydrogels with intervening external forces were immersed in ferric chloride solution. With the increase of time, the hydrogels changed from colorless and transparent to dark yellow. At this time, ionic coordination bonds were formed between Fe^{3+} and the carboxyl groups of AAc and CCNFs through supramolecular metal ion-carboxyl complexation, forming a tighter network with stronger mechanical properties. Thus P(AAc-co-AAm)/CCNFs-Fe^{3+} hydrogels with secondary cross-linked networks were formed. Finally, the above hydrogels were unloaded and washed with deionized water to prevent further compounding reactions. In this study, double cross-linked hydrogels with different CCNFs contents of 0 wt.%, 1 wt.%, 2 wt.%, and 3 wt.% were prepared. The ingredients used were formulated, as shown in Table S1 in the Electronic Supplementary Material (ESM). When the CCNFs content exceeded 3 wt.%, the pre-polymerization solution became so thick that it was impossible to prepare hydrogels with homogeneous composition. CCNFs are expected to significantly enhance the mechanical properties of the hydrogels due to their large aspect ratio and excellent mechanical properties. Also, due to the large number of carboxyl groups on CCNFs, the formation of coordination bonds between carboxyl groups and metal ions can improve shape memory properties of hydrogels [39, 40]. The elastic potential energy stored in the pre-stretched hydrogel can allow for energy conversion during the deformation process and thus a greater burst of driving energy.

In order to observe the surface micromorphological structures of composite hydrogels with different compositions, scanning electron microscopy was used to observe P(AAc-co-AAm), 3 wt.% P(Aac-co-Aam)/CCNFs, P(Aac-co-Aam)/CCNFs-Fe^{3+}, and light-reduced P(AAc-co-AAm)/CCNFs-Fe^{2+} hydrogels, after swelling and freeze-drying (Fig. S1 in the ESM). It can be seen that the pore size of the P(AAc-co-AAm) hydrogel without CCNFs after 10 min of swelling was approximately 3–5 μm. The pore size was homogeneous with uniformly distributed. The 3 wt.% P(AAc-co-AAm)/CCNFs hydrogels produced larger pore sizes than those without fibers. The pore size was more homogeneous, ranging from 5 to 13 μm. This is due to the fact that the stronger stiffness provided by the addition of CCNFs to the hydrogel can support the flexible P(AAc-co-AAm) polymer chains and avoid severe shrinkage during the freeze-drying process. For P(AAc-co-AAm)/CCNFs-Fe^{3+} hydrogels, the ionic coordination formed by the large number of carboxyl groups in the P(AAc-co-AAm)/CCNFs system with Fe^{3+} results in a tighter cross-linked network of the hydrogels. The pore size (300 nm–3 μm) was greatly reduced compared with that before coordination, which was conducive to achieving stronger mechanical properties. When the Fe^{3+} in the network was reduced to Fe^{2+} by UV light, the ion-coordination bonds were greatly reduced or even returned to the original state, which made the hydrogels return to a loose state. Therefore, it can be seen that the pore size distributions of both P(AAc-co-AAm)/CCNFs-Fe^{2+} and 3 wt.% P(AAc-co-AAm)/CCNFs hydrogels was similar and the pore size were very close. In addition, the SMCH before and after photo-reduction was observed by X-ray energy spectroscopy analysis (Fig. S1 in the ESM). Although less iron was present in the reduced gel system and divalent iron was involved in complexation with carboxyl groups to some extent, we believed that light was an effective way to weaken or even eliminate the coordination bonds in the system.

To investigate the interactions between different components in the hydrogel system, CCNFs, different ratios of P(AAc-co-AAm)/CCNFs (0 wt.%, 1 wt.%, 2 wt.%, and 3 wt.%) and 3 wt.% P(AAc-co-AAm)/CCNFs-Fe^{3+} hydrogels were characterized by infrared spectroscopy (Fig. S2 in the ESM). The CCNFs spectra showed a hydroxyl peak at 3407 cm^{-1} for intermolecular hydrogen

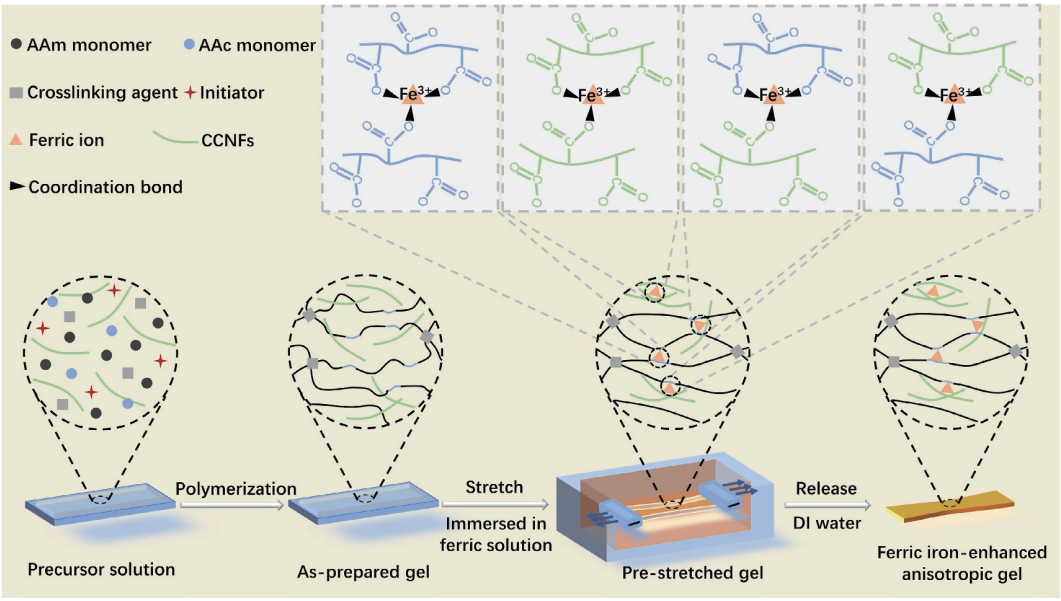

Figure 1 Schematic diagram of the fabrication of pre-stretched SMCH.

bonding, indicating that the addition of CCNFs increased the non-covalent interactions of the system. Meanwhile, the asymmetric stretching band and symmetric stretching band produced by the carboxylic acid groups of CCNFs presented at 1605 and 1423 cm^{-1}, respectively [41, 42]. In the P(AAc-co-AAm) gel spectrum, the N–H stretching vibration belonging to AAm was detected at 3352 cm^{-1}. The stretching vibrations of carbonyl C=O and N–H of the amide I band were detected at 1664 and 1612 cm^{-1}, respectively. Compared with P(AAc-co-AAm), the characteristic peaks of the spectra of P(AAc-co-AAm)/CCNFs and P(AAc-co-AAm)/CCNFs-Fe^{3+} were both red-shifted at the position of 3352 cm^{-1}, which was attributed to the non-covalent bonding interactions between CCNFs and P(AAc-co-AAm), such as hydrogen bonding and van der Waals forces. However, the positions of the other characteristic peaks of P(AAc-co-AAm)/CCNFs and P(AAc-co-AAm)/CCNFs-Fe^{3+} did not change significantly, which may be due to the overlap of the characteristic peaks of CCNFs with those associated with P(AAc-co-AAm). In addition, no new vibrational absorption peaks appeared on the P(AAc-co-AAm)/CCNFs and P(AAc-co-AAm)/CCNFs-Fe^{3+} spectra, indicating that no new chemical functional groups were formed in these two composite hydrogels.

3.2 Mechanical properties of hydrogels

Excellent mechanical properties are important for shape memory hydrogels applications. Tensile experiments were performed to determine whether the addition of CCNFs and the effect of Fe^{3+} would change the strength of the hydrogels. Figure 2 shows the tensile data of P(AAc-co-AAm)/CCNFs and P(AAc-co-AAm)/CCNFs-Fe^{3+} hydrogels with different CCNFs contents. For the P(AAc-co-AAm)/CCNFs hydrogels, the mechanical properties were strongly dependent on the CCNFs content. As the CCNFs content increased, the elongation at break kept decreasing, while the maximum tensile strength kept increasing. Compared with the hydrogel without CCNFs, the elongation at break of the 3 wt.% hydrogel was reduced by 45% (~ 500%), but its strength was increased by 120% (~ 0.16 MPa) (Figs. 2(a) and 2(c)). The stress–strain curves reflect the elastic deformation properties of the hydrogels. Quantification with tensile modulus revealed that the value of Young's modulus was positively correlated with the content of fibers (Fig. 2(b)), indicating that the incorporation of CCNFs effectively increased the energy dissipation of the gel system. The hydrogen bonding interactions generated by the large number of hydroxyl groups on the fibers in the hydrogel network could act as sacrificial bonds to protect the copolymers of the main chain during crack propagation. After chelation of Fe^{3+}, the orientation of the fiber and polymer chains in the pre-stretched gel network was locked to some extent by metal coordination and produced a second level of tighter cross-linking, resulting in more robust mechanical properties. The hydrogel with 3 wt.% content, for example, showed a significant increase in tensile strength of 8.7 times (~ 1.55 MPa) compared with the hydrogels without Fe^{3+} addition, but a 68% (~ 160%) reduction in elongation at break (Figs. 2(e) and 2(g)). At the same time, the tensile modulus of P(AAc-co-AAm)/CCNFs-Fe^{3+} hydrogels was significantly improved up to 1.51 MPa, which is 437.6% higher compared with 3 wt.% P(AAc-co-AAm)/CCNFs hydrogels (Fig. 2(f)). Such mechanical properties were able to meet the needs of bionic deformable materials. These effects could be attributed to the strong interactions of supramolecular coordination bonds formed by iron and carboxyl groups in the hydrogel network. During the stretching process, stresses were transferred from the polymer chains to the cross-linked sites with iron ions and spread along their longitudinally ordered direction relative to the pre-stretching, instead of being torn in the transverse direction. At the same time, the fracture and reformation of the interaction of the iron ions and the carboxyl groups enabled them to effectively prevent fracture at higher stresses. Schematic diagrams of the stretching of the two component hydrogels are shown in Figs. 2(d) and 2(h).

3.3 Shape memory properties

The reversible transformation of metal-ligand coordination provides a reliable shape memory function for hydrogels. To investigate the effect of CCNFs addition on the effect of hydrogel shape memory, shape memory properties of hydrogels with different CCNFs contents at 150% strain were characterized in terms of SFR after immersion in 0.1 M $FeCl_3$ for different time on 3D printed molds, as shown in Fig. 2(i). The SFR was strongly dependent on the content of CCNFs, especially in the early stage of hydrogels and metal ion interaction. At 10 min of immersion, the SFR of the hydrogels increased with increasing CCNFs content. The hydrogels with 3 wt.% CCNFs showed an SFR of 77.8%, higher than either group, and 27.4% higher than that of the group without CCNFs. The iron chelation rate of the hydrogel system gradually slowed down and finally stabilized as the soaking time increased. The SFR reached more than 90% at 40 min. At

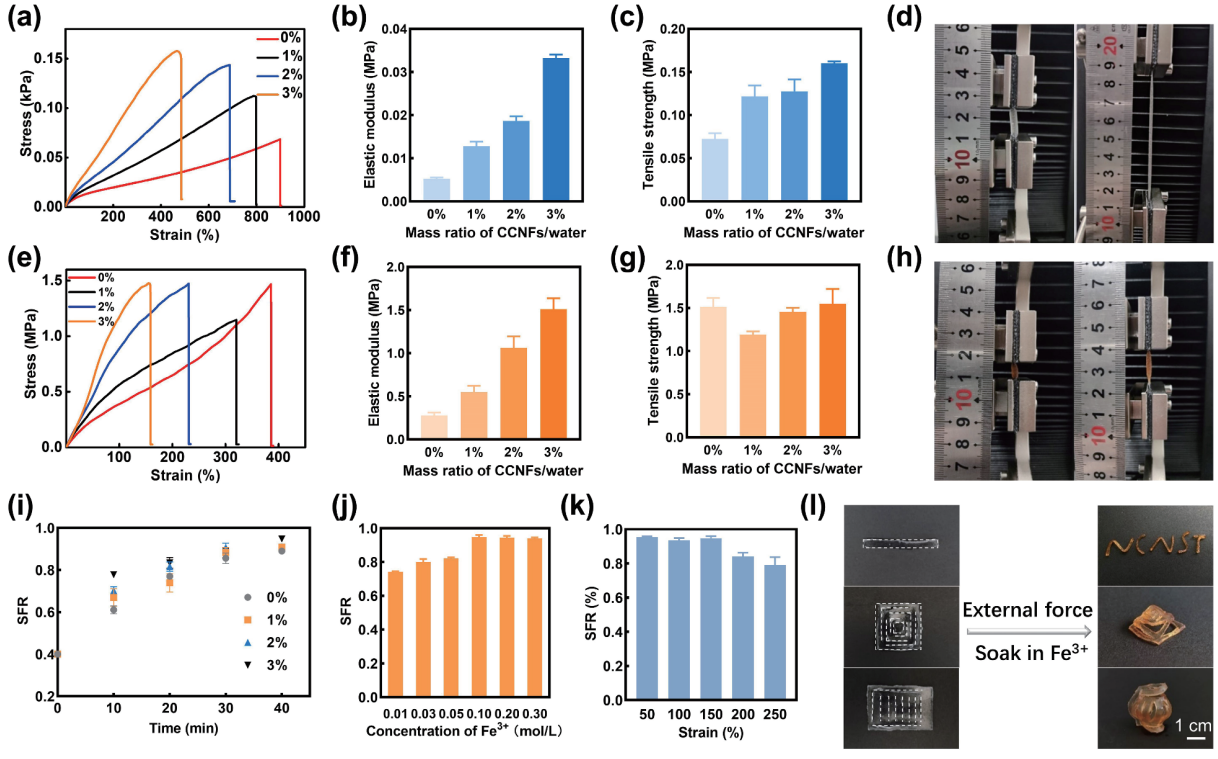

Figure 2 Mechanical property tests and shape memory properties. (a) Stress–strain curves of P(AAc-co-AAm)/CCNFs hydrogels with different CCNFs contents. (b) Elastic modulus of P(AAc-co-AAm)/CCNFs hydrogels with different CCNFs contents. (c) Maximum tensile strength of P(AAc-co-AAm)/CCNFs hydrogels with different CCNFs contents. (d) Images of P(AAc-co-AAm)/CCNFs hydrogels before and after stretching. (e) Stress–strain curves of P(AAc-co-AAm)/CCNFs-Fe^{3+} hydrogels with different CCNFs contents. (f) Elastic modulus of P(AAc-co-AAm)/CCNFs-Fe^{3+} hydrogels with different CCNFs contents. (g) Maximum tensile strength of P(AAc-co-AAm)/CCNFs-Fe^{3+} hydrogels with different CCNFs contents. (h) Images of P(AAc-co-AAm)/CCNFs-Fe^{3+} hydrogels before and after stretching. (i) SFR of hydrogels with different CCNFs contents at different immersion time. (j) Shape fixation rates of hydrogels soaked with different concentrations of Fe^{3+}. (k) Shape fixation rate of hydrogels with different stretching strains. (l) Demonstration of shape memory function. Changing the hydrogel from 1D to 2D state and from 2D to 3D state by applying external force and immersing in Fe^{3+} solution.

this point, although the SFR was very close, its magnitude was still positively correlated according to the concentration of CCNFs as in the previous time. The SFR of the 3 wt.% hydrogel was still higher than the other three groups, reaching 94.8%, and was 6.5% higher than that of the group without CCNFs. The above results indicated that the higher content of CCNFs had faster chelation of Fe^{3+} and more stable immobilization. This coincided with the idea that the addition of CCNFs not only enhanced the mechanical properties of P(AAc-co-AAm) hydrogels, but also improved the speed and effectiveness of shape fixation by increasing the carboxyl group content in the gel system. In addition to the two factors of CCNFs content and time, the concentration of Fe^{3+} and the percentage of pre-stretching also affect the shape memory effect. The SFRs were measured after 40 min of interaction with the Fe^{3+} solution at different Fe^{3+} concentrations (0.01, 0.03, 0.05, 0.10, 0.20, and 0.30 M) and different stretching strains (50%, 100%, 150%, 200%, and 250%) (Figs. 2(j) and 2(k)). Among them, the percentage of stretching of the hydrogels in Fig. 2(j) is 150%, while the Fe^{3+} immersion concentration of the hydrogels in Fig. 2(k) is 0.10 M. It is easy to know that the SFR increased with increasing Fe^{3+} concentration until the Fe^{3+} concentration reached 0.10 M, where it did not increase anymore or even there was a certain tendency to decrease. This could be attributed to the fact that sufficient Fe^{3+} was required for ionic cross-linking. Ideally, three iron ions were required to coordinate each carboxyl group, so higher concentrations of the solution had a large amount of Fe^{3+} penetrating into the hydrogels and achieving better fixation, with only little relaxation after being released. Similarly, the SFR of the hydrogels was essentially equal when it was stretched by 50%–150% of its length. The decrease in SFR at a stretching percentage above 200% was due to the fact that the current experimental parameters did not support the storage of elastic potential energy corresponding to higher stretching strains, resulting in a relatively large retraction of the pre-stretched hydrogel after release. Therefore, the minimum Fe^{3+} concentration that could maintain a good shape memory effect under this experimental condition was 0.10 M and the maximum stretching strain was 150%. In addition, different shapes could be formed by fusing the tailor-programmed one- or two-dimensional (1D or 2D) hydrogels under external forces and releasing them after immersion in $FeCl_3$ solution for a period of time. For example, several one-dimensional striped hydrogels were fixed as the logo of this research unit "NCNST", and two-dimensional Chinese character "Hui" type hydrogels and striped patterned hydrogels were fixed as three-dimensional buildings and lantern shapes (Fig. 2(l)).

3.4 Solvent-induced shape deformation of metal ion programmed hydrogels

In addition to the shape memory properties, we also investigated the behavior of hydrogels programmed with metal ions under solvent induction. First, the swelling behaviors of P(AAc-co-AAm)/CCNFs, P(AAc-co-AAm)/CCNFs-Fe^{3+}, and P(AAc-co-AAm)/CCNFs-Fe^{2+} hydrogels after light reduction were observed (Fig. S3 in the ESM). All three hydrogels reached the swelling equilibrium at hour 24. The gel network of P(AAc-co-AAm)/CCNFs-Fe^{3+} became very tight and less swollen due to the good coordination of iron ions. Its significant difference in swelling from the other two groups of hydrogels would be quite favorable for constructing differentially swollen hydrogels programmed by metal ions. The key to achieving the solvent-induced deformation behavior of metal ion programmed

hydrogels is the inhomogeneous introduction of metal ligand structures into the hydrogels. Compared with the unchelated Fe^{3+} site, the chelated Fe^{3+} site had a more dense hydrogel cross-linked network due to the formation of the metal ligand structure. From the swelling experiments, it was known that the two had different degrees of swelling after free swelling in water, and this difference in swelling led to the generation of in-plane stresses in the hydrogel, causing bending or deformation of the hydrogel. The driving force for this deformation was the osmotic pressure difference between the hydrogel and the surrounding solvent. Specifically, the degree of swelling of the part programmed by metal ions was lower than that of the part not programmed. After free swelling in water, the volume change of the programmed part was much smaller than that of the unprogrammed part, resulting in the corresponding hydrogel deformation phenomenon. In addition, thickness plays a crucial role in the actuation effect of water permeation-dependent drivable hydrogels. The bending angles of P(AAc-co-AAm)/CCNFs hydrogels with different thicknesses after being coated unilaterally by Fe^{3+} solutions at different time were explored (Fig. 3(a)). The bending angles of the hydrogels showed a clear time dependence and thickness dependence. The time dependence was still attributed to the longer time required for the complexation of iron ions with carboxyl groups before the reaction reached equilibrium. The actuation of the hydrogel did not work when the mismatch stress due to the difference in swelling was not sufficient to allow the thicker hydrogel to overcome the in-plane stress bending. Thus the 1 mm thick hydrogels showed good bending deformability, which reached a bending angle of 644° after 7 min of action with iron, 63.0% higher than that of the 2 mm thick hydrogel. The bending angle-time curve obtained by immersing a 1 mm thick hydrogel coated with 0.1 M Fe^{3+} on one side for 5 min in 0.3 M EDTA for reduction is shown in Fig. 3(b). It was easy to see that the hydrogel took several minutes to complete the metal ion programming, and the time required to remove the programming using metal chelator was about 13 min. Figure 3(c) presents the diffuse reflectance UV–Vis spectra of the hydrogels at different reduction time points. The curves showed that the absorption intensity of the hydrogel gradually decreased with the increase of the EDTA reduction time. It indicated that the Fe^{3+} in the hydrogel could be reversibly reduced or eliminated by the chelator, further demonstrating the reproducible programming nature of SMCH. The bending angle-time diagram was derived by cycling the hydrogel in water-anhydrous ethanol after applying 0.1 M Fe^{3+} solution to one side of the hydrogel (Fig. 3(d)). The hydrogel bent toward the Fe chelate side in water due to the difference in swelling properties. The hydrogels recovered to a state close to the pre-swelling state after immersion in anhydrous ethanol. This is due to the fact that the solubility of PAAc and PAAm in ethanol is much less than that in water. A small amount of anhydrous ethanol displaced a large amount of water from the hydrogel and then evaporated rapidly in air to make the hydrogel eliminate swelling rapidly. The bending angle of the hydrogel showed a slow increase with the increase of cycles after 5 cycles of alternating between water and ethanol, which was caused by the swelling behavior of the hydrogel accumulated in several cycles, and the replacement effect of anhydrous ethanol was not thorough enough. However, the hydrogel angles in water or anhydrous ethanol were still limited to their respective ranges and well distinguished, which proved that water and anhydrous ethanol could be used as effective solvents for reversible actuation of hydrogels, providing a reliable reference for irreversible shape

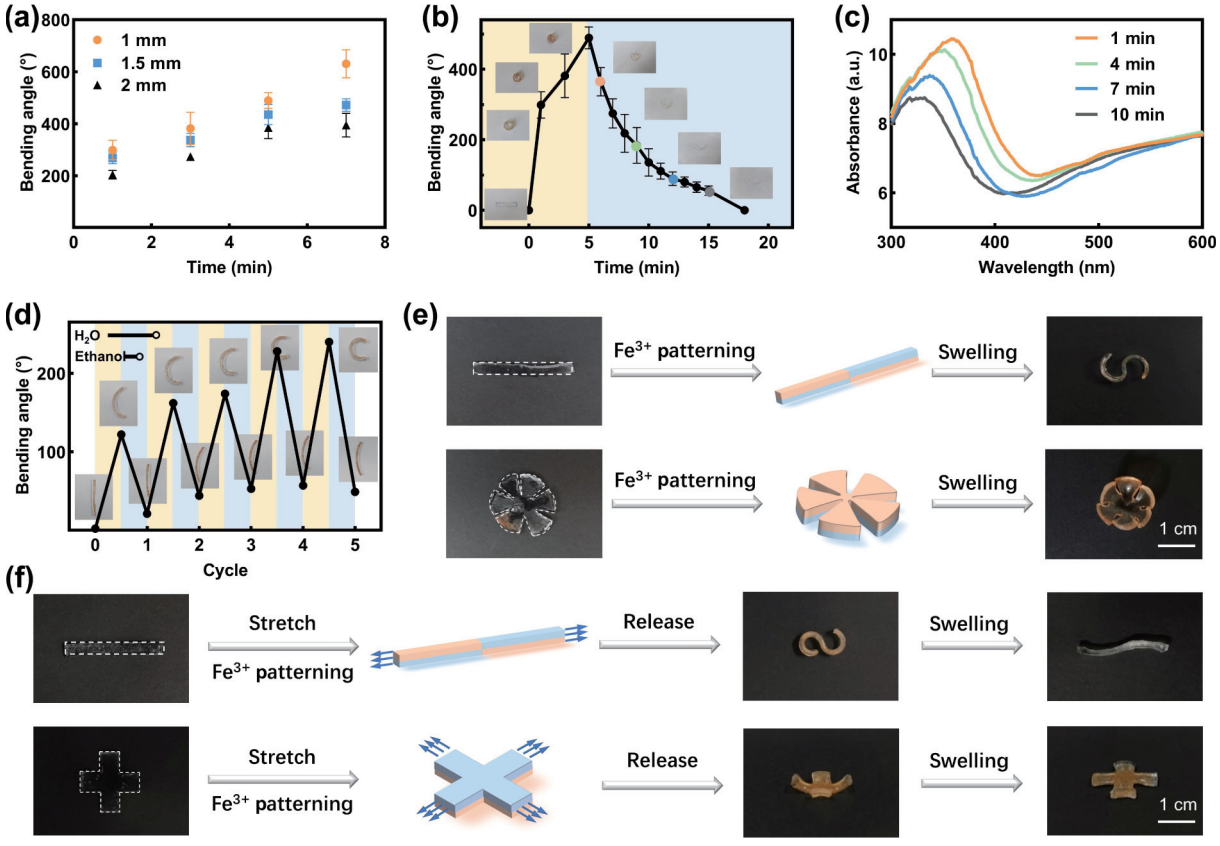

Figure 3 Solvent-induced deformation of metal ion programmed hydrogels. (a) Bending angles for different thicknesses of hydrogels coated with Fe^{3+} on one side for different time. (b) Bending angle–time curves of 1 mm thickness hydrogels coated with 0.1 M Fe^{3+} for 0–5 min on one side and immersed in 0.3 M EDTA. (c) Diffuse reflectance UV–Vis spectra of hydrogels at different reduction time. (d) Stability cycling test for reversible actuation of the solvent. Bending angle–time curves of hydrogels placed in water-ethanol for 5 alternating cycles after coating with 0.1 M Fe^{3+}. (e) Shape deformation of metal ion programmed hydrogels by solvation mismatch. (f) Shape deformation process of pre-stretched metal ion hydrogel produced first by strength mismatching and then by swelling mismatching.

memory hydrogel ground actuation. Figures 3(e) and 3(f) demonstrate the shape deformation behavior of metal ion programmed hydrogels by water swelling. Based on the swelling mismatch, the hydrogel patterned by metal ions transformed from a one-dimensional strip to a positive "S" shape after swelling, and transformed from a two-dimensional flat flower to a three-dimensional flower (Fig. 3(e)). The hydrogels were pre-stretched and programmed by metal ions with different deformation paths (Fig. 3(f)). After being pre-stretched and programmed by metal ions, the metal chelated regions had a higher crosslink density and strength, and the non-chelated regions were relatively soft. Based on the strength mismatch principle, the release caused the gel to bend toward the non-chelated side. Therefore, the pre-stretched programmed hydrogel changed from a one-dimensional linear shape to a two-dimensional inverse "S" shape after release, and the opposite tendency of bending motion to a positive "S" shape after solubilization. The hydrogel bent from the Chinese character "ten" to the non-chelated side to form a gripper shape, and the opposite bending motion tended to bend to the chelated side after dissolution.

The above-mentioned reversible solvent and metal ion programming were used to design a dynamic demonstration of hydrogel deformation behavior. First, the patterns and simulation effects of the iron ion programmed hydrogel were designed (Figs. 4(a) and 4(b)). Figure 4(c) shows the programmed hydrogel swelling in water to form a helical shape driving the propeller to rotate clockwise (Figs. 4(c)(i) and 4(c)(ii)) and deconvolving in EDTA solution driving the propeller to rotate counterclockwise (Figs. 4(c)(iii) and 4(c)(iv)) (Movie ESM1). The process of programmed hydrogels to swell in water to simulate flower closure (Figs. 4(d)(i) and 4(d)(ii)) and deswelling in anhydrous ethanol and air to simulate flower opening (Figs. 4(d)(iii) and 4(d)(iv)) is illustrated in Fig. 4 (Movie ESM2). Although this deformation cycle could not be repeatedly actuated without external loading, its reproducible programmability was still practical. The original hydrogel was programmed with different patterns (e.g., stripes, diagonals, and squares) by the trivalent iron solution in three different deformation cycles, and was transformed into the corresponding three-dimensional shape after swelling (Fig. 4(e)), which well demonstrated the reprogrammability and reusability of SMCH.

3.5 UV light-induced deformation of shape memory hydrogels

However, the solvent effect of hydrogels is usually considered slow due to the dependence on the diffusion rate, as confirmed in Section 3.4. And shape memory hydrogels are of irreversible deformation type, supramolecular metal-ligated shape memory hydrogels store strong elastic potential energy by pre-stretching techniques that need to be designed for efficient energy conversion. Therefore, there is an urgent need for optical programming to be introduced to achieve complementary effects with metal ion programming. The formation of shape memory hydrogels by metal ion coordination of hydrogels and their reduction by UV light is shown in Fig. 5(a). The cross-link density of the hydrogel network increased due to the coordination of Fe^{3+} resulting in strong mechanical properties. The hydrogel remained horizontal under the condition of gravity. Since the binding affinity between Fe^{2+} and carboxyl groups is much less than that of Fe^{3+}, the coordination bond between Fe^{3+} and the carboxyl groups provided in the hydrogel network dissociated after the reduction

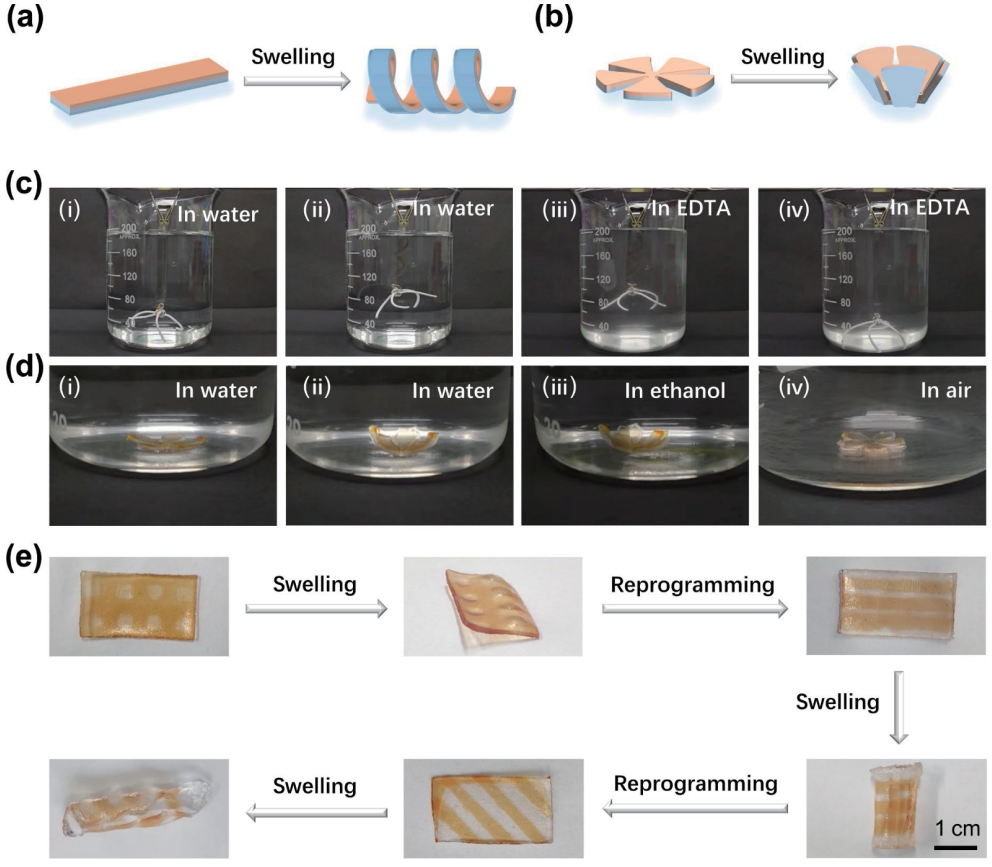

Figure 4 Demonstration of deformation behavior of hydrogel programmed by solvent-induced metal ions. (a) Schematic diagram of programmed hydrogel deformation for simulating propeller. (b) Schematic diagram of programmed hydrogel deformation simulating flower opening and closing. (c) Simulation of propeller rotation: (i) initial state of immersion in water, (ii) curling in water, (iii) initial state of immersion in EDTA, and (iv) recovery of shape in EDTA. (d) Simulation of flower opening and closing: (i) initial state of immersion in water, (ii) closing in water, (iii) initial state of immersion in anhydrous ethanol, and (iv) opening in anhydrous ethanol and air. (e) Reproducible programmability.

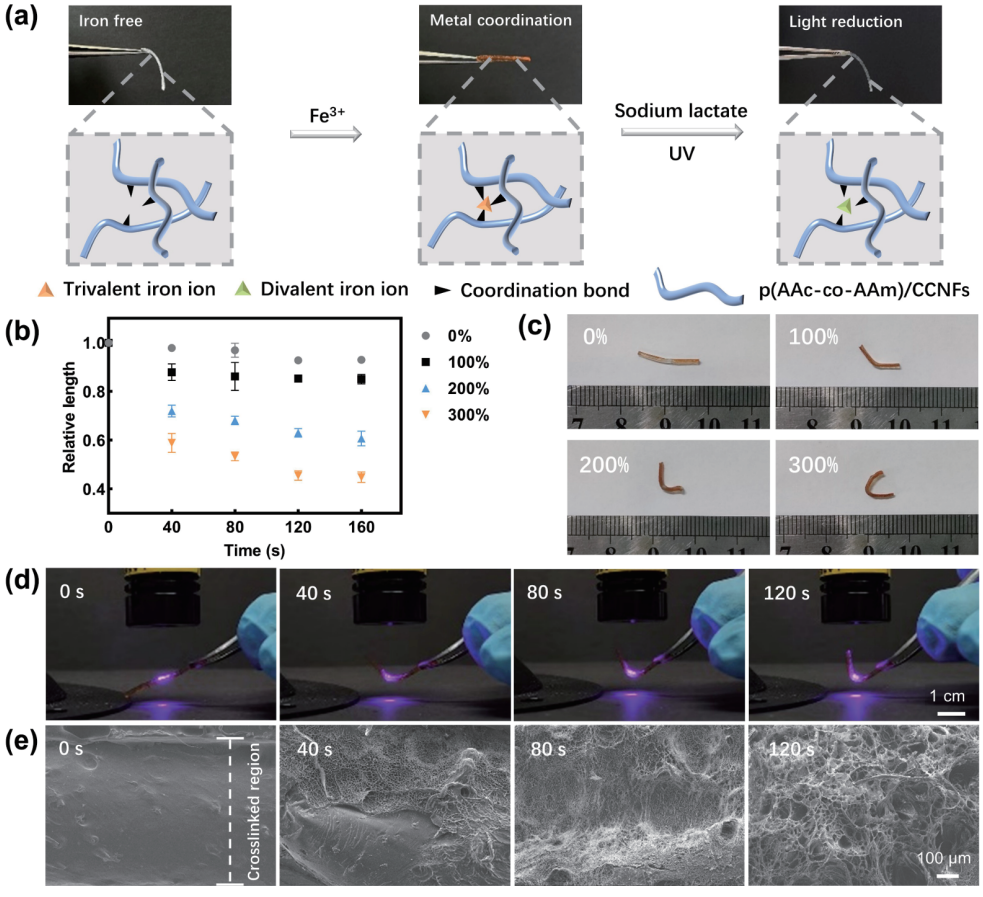

Figure 5 Light-induced deformation of hydrogels. (a) Schematic diagram of the working of the photoresponsive hydrogel. (b) Bending degree of hydrogels with different tensile strains at different light stimulation time (the relative length is the ratio of the distance between the two endpoints after illumination and the initial). (c) Effect of stretching strains on the effect of light reduction. Graph of bending effect after light reduction for hydrogels with 0%, 100%, 200%, and 300% stretching. (d) Bending effect of UV light irradiation at different time with fixed stretching strain (300%). (e) SEM comparison of illuminated and unilluminated layers.

of Fe^{3+} to Fe^{2+} by UV light, leading to the stress relaxation of the hydrogel. The reduced hydrogel returned to its pre-coordination state and became soft. This change in stiffness made possible the deformation caused by intensity mismatch due to fixed-point illumination. First, the degree of bending deformation of hydrogels with different stretching strains under different light stimulation time was investigated, and the relative length was used to measure the degree of deformation (Fig. 5(b)). In agreement with the expected results, the fixed-point light exposure did lead to the bending and deformation of the hydrogel. This was because at the light locus, the lighted side was reduced to become soft while the other side remained in its initial hard state. The strength mismatch led to an asymmetric release of stress and the bending phenomenon. The pre-stored elastic potential energy in the hydrogel was converted into mechanical energy during this process. The trend of each data point showed that the bending deformation rate of the hydrogel became slow from fast. The degree of deformation increased with increasing time of the light stimulation. The deformation rate was the fastest during the first 40 s, and the degree of bending almost stopped increasing by 160 s. Therefore, we took 120 s as the time required to complete the maximum degree of deformation. The degree of bending became significantly greater with increasing stretching strain over the range of 0%–300% stretching strain. The degree of deformation increased with the percentage of stretching. The relative length at 300% stretch was only 0.45, which was 47.0% lower compared with 100% stretch and 51.6% lower compared with unstretched. This demonstrated that the pre-stretching percentage determined the magnitude of the stored elastic potential energy of the supramolecular shape memory hydrogel, which ultimately affected the degree of bending deformation produced by the fixed-point light. The bending deformation processes of the hydrogels with different tensile strains and 300% tensile strains within 120 s of light stimulation are shown in Figs. 5(c) and 5(d) (Movie ESM3). The hydrogel could produce significant bending deformation within 40 s and reach the maximum bending degree at 120 s. To further verify that the chelated Fe^{2+} in the hydrogel was gradually reduced during the light exposure, the apparent morphology is analyzed for different light exposure time in Fig. 5(e). The hydrogel network was tightly cross-linked and no pores were found at the initial moment. With time increasing, a clear reduction region could be observed in the vertical direction with pore generation. The reduction zone extended from 1/2 to about 4/5 in the time period of 40 to 80 s. The reduction of the hydrogel surface was essentially complete and the pore size became more pronounced by 120 s. These results indicated that combining pre-stretching with spot lighting was an effective response for supramolecular metal-liganded shape memory hydrogels, which effectively utilized energy conversion and was faster, more efficient, and more powerful than the solvent response.

3.6 UV light programming induces deformation of supramolecular shape memory hydrogels for applications

It has been demonstrated that light could induce a corresponding deformation of the hydrogel by programming its reduction sites. Based on this, the demonstration of its application was performed. The hydrogel hooks formed by bending a straight hydrogel after spot illumination could hook up and transfer the white wood to another position, as shown in Fig. 6(a) (Movie ESM4). Light

reduction of the pre-stretched weight-bearing hydrogel in the vertical direction caused the gel to contract and enabled lifting of heavy objects. Figure 6(b) shows that the hydrogel lifted a 1.3 g dovetail clip vertically upward by a height of 4 mm after 2 min of UV light irradiation (Movie ESM5), similar to the contraction and pulling of muscles. The above demonstration proved that the pre-stretched supramolecular shape memory hydrogel could perform mechanical work under light induction to achieve bending, contraction, and weight-bearing. In addition, the pre-stretched SMCH could be constructed into more complex shape deformations by taking advantage of the UV light's ability to be programmed at a fixed point. The corresponding design is shown in Fig. 6(c), where the direction of the purple arrow indicated the direction of the light. For example, a one-dimensional pre-stretched strip hydrogel was induced into a two-dimensional triangular shape by UV light programming of the reduction sites. The reduction sites of the pre-stretched cross hydrogels in four directions were programmed and induced by light to eventually become interesting three-dimensional insect water striders. However, although the pre-stretched SMCH could be applied for mechanical work and shape programming, essentially no real actuation was still achieved, as it could only function in one deformation cycle. For this reason, the light-induced pre-stretched SMCH was eventually combined with a solvent-responsive approach, where two independent response mechanisms could be programmed during the deformation of the hydrogel without interfering with each other. The specific procedure is shown in Fig. 6(d). First, the P(AAc-co-AAm)/CCNFs hydrogels were prepared as SMCH using the pre-stretching technique. Subsequently, the hydrogels were deformed by light local reduction, while the overall reduction restored the hydrogels to their original soft state. Finally, soaking the partially reduced hydrogels in different solvents alternately enabled cyclic driving without the need to load a new deformation cycle by external forces. This study truly realized the organic combination of shape memory and actuation. By simulating the reversible manipulation of the hand, we demonstrated the above programmed deformation process (Fig. 6(e)). Four longer fingers were bent one by one under light (Figs. 6(e)(i)–6(e)(iv)) to make the unfolded palm into a clenched fist. By swelling the fist in water, the fingers created a tendency to bend toward the unreduced side due to the higher degree of swelling on the light-reduced side than on the unlighted side, thus unfolding the fist to some extent (Fig. 6(e)(v)). When it was swollen in anhydrous ethanol, the local reduction site was eliminated from swelling due to the displacement and strong volatilization effect of ethanol, leading to the restoration of finger bending (Fig. 6(e)(vi)). So repeatedly swelling in water (Fig. 6(e)(vii)) and ethanol (Fig. 6(e)(viii)), the finger unfolding and bending were reversible. The feasibility of programmed deformation was demonstrated and provided a strong reference for reversible driving of shape memory hydrogels.

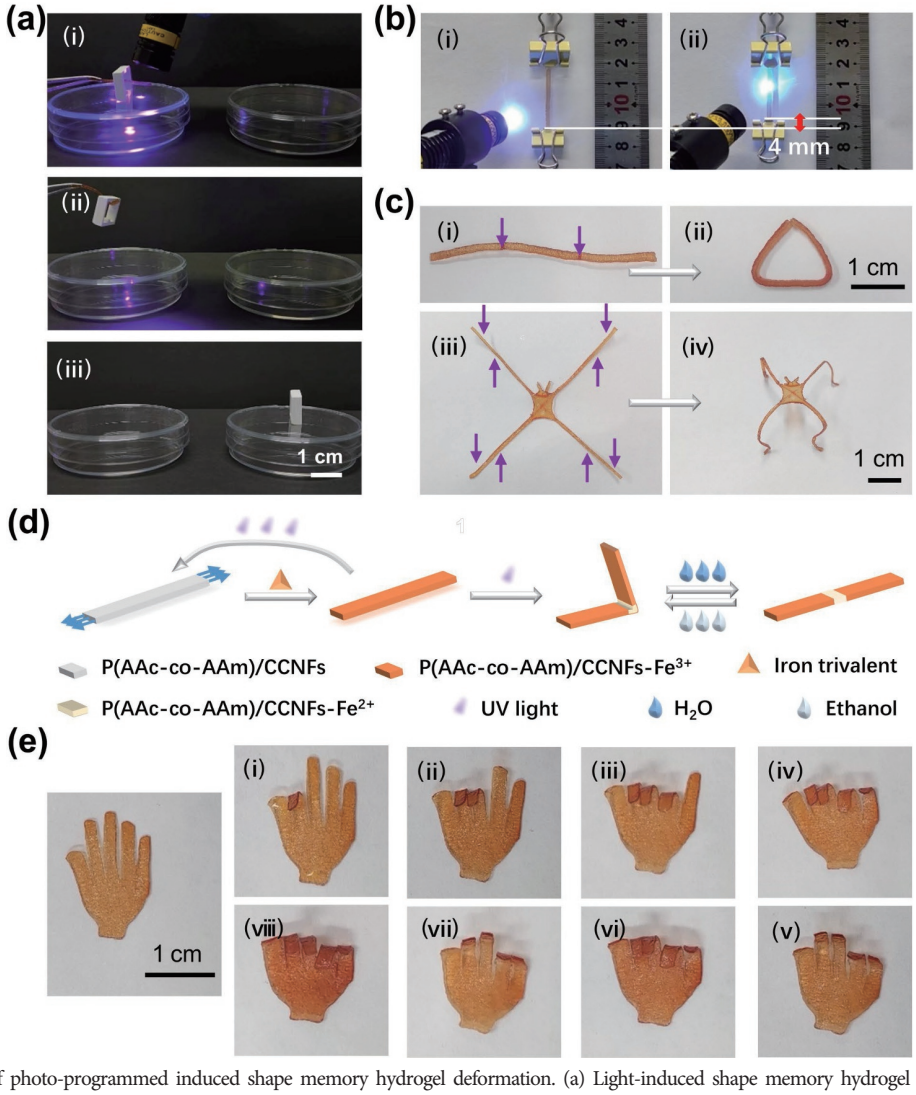

Figure 6 Application of photo-programmed induced shape memory hydrogel deformation. (a) Light-induced shape memory hydrogel hooking and moving an object. (b) Light-induced shape memory hydrogel lifting an object vertically. (c) UV light shape programming of hydrogels. (d) Schematic diagram of the principle of programmed deformation. (e) Programmed deformation produced by the combination of light programming and solvent response.

4 Conclusions

In conclusion, a pre-stretched supramolecular metal-liganded shape memory hydrogel P(AAc-co-AAm)/CCNFs-Fe^{3+} was successfully constructed for programable actuator. The hydrogels represent excellent mechanical properties and strong deformation performance. The prepared hydrogels respond to solvent and light independently. The difference in cross-link density due to swelling mismatch and metal ion chelation imparts the hydrogel solvent-responsive properties. By metal ion programming, the hydrogels exhibit reversible deformation patterns in water-ethanol solutions, such as flower opening and closing. Photo irradiation induces intensity mismatch in pre-stretched shape memory hydrogels, enabling rapid and programable diverse shape deformation behaviors such as mechanical work and programmed deformation of two- or three-dimensional shapes. The reconfigurability of hydrogels is expected to enable recycling of hydrogels in industrial production. More importantly, light induced pre-stretched supramolecular metal-ligand hydrogels and the intervention of different kinds of solvents enable complex reversible programmed deformations, such as the bending and unfolding of fingers. In addition, the potential coupling effects in the dual response actuation process are key to understanding the overall behavior and performance of this hydrogel system. In the future, we will also observe the actuation response of the hydrogels by computer simulations or by systematically varying the experimental conditions of the stimulus response to quantify the possible coupling effects. The combination of these two deformation modes, shape memory, and actuation, successfully transforms the hydrogel's own deformation behavior into motion behavior, providing a good model for programmed deformation of hydrogel actuators.

Acknowledgements

This research was funded supported by the Key Research Program of Frontier Sciences of CAS (Nos. ZDBS-LY-SLH036 and QYKJZD-SSW-SLH02).

Electronic Supplementary Material: Supplementary material (formulation of hydrogels, SEM and EDS analysis plots, infrared spectroscopy analysis, swelling rate, and Movies ESM1–ESM5) is available in the online version of this article at https://doi.org/10.1007/s12274-023-5948-8.

References

[1] Dawson, C.; Vincent, J. F. V.; Rocca, A. M. How pine cones open. *Nature* **1997**, *390*, 668.

[2] Armon, S.; Efrati, E.; Kupferman, R.; Sharon, E. Geometry and mechanics in the opening of chiral seed pods. *Science* **2011**, *333*, 1726–1730.

[3] Liu, Z. Q.; Jiao, D.; Zhang, Z. F. Remarkable shape memory effect of a natural biopolymer in aqueous environment. *Biomaterials* **2015**, *65*, 13–21.

[4] Sullivan, T. N.; Zhang, Y. L.; Zavattieri, P. D.; Meyers, M. A. Hydration-induced shape and strength recovery of the feather. *Adv. Funct. Mater.* **2018**, *28*, 1801250.

[5] Tang, L.; Wang, L.; Yang, X.; Feng, Y. Y.; Li, Y.; Feng, W. Poly(N-isopropylacrylamide)-based smart hydrogels: Design, properties and applications. *Prog. Mater. Sci* **2021**, *115*, 100702.

[6] Ko, B.; Badloe, T.; Yang, Y.; Park, J.; Kim, J.; Jeong, H.; Jung, C.; Rho, J. Tunable metasurfaces via the humidity responsive swelling of single-step imprinted polyvinyl alcohol nanostructures. *Nat. Commun.* **2022**, *13*, 6256.

[7] Dong, Y.; Wang, J.; Guo, X. K.; Yang, S. S.; Ozen, M. O.; Chen, P.; Liu, X.; Du, W.; Xiao, F.; Demirci, U. et al. Multi-stimuli-responsive programmable biomimetic actuator. *Nat. Commun.* **2019**, *10*, 4087.

[8] Zhu, C. N.; Li, C. Y.; Wang, H.; Hong, W.; Huang, F. H.; Zheng, Q.; Wu, Z. L. Reconstructable gradient structures and reprogrammable 3D deformations of hydrogels with coumarin units as the photolabile crosslinks. *Adv. Mater.* **2021**, *33*, 2008057.

[9] Qin, J. J.; Chu, K. B.; Huang, Y. P.; Zhu, X. M.; Hofkens, J.; He, G. J.; Parkin, I. P.; Lai, F. L.; Liu, T. X. The bionic sunflower: A bio-inspired autonomous light tracking photocatalytic system. *Energy Environ. Sci.* **2021**, *14*, 3931–3937.

[10] Jiang, Z.; Tan, M. L.; Taheri, M.; Yan, Q.; Tsuzuki, T.; Gardiner, M. G.; Diggle, B.; Connal, L. A. Strong, self-healable, and recyclable visible-light-responsive hydrogel actuators. *Angew. Chem., Int. Ed.* **2020**, *59*, 7049–7056.

[11] Li, C.; Xue, Y. G.; Han, M. D.; Palmer, L. C.; Rogers, J. A.; Huang, Y. G.; Stupp, S. I. Synergistic photoactuation of bilayered spiropyran hydrogels for predictable origami-like shape change. *Matter* **2021**, *4*, 1377–1390.

[12] Zhu, Q. L.; Dai, C. F.; Wagner, D.; Daab, M.; Hong, W.; Breu, J.; Zheng, Q.; Wu, Z. L. Distributed electric field induces orientations of nanosheets to prepare hydrogels with elaborate ordered structures and programmed deformations. *Adv. Mater.* **2020**, *32*, 2005567.

[13] Lee, Y. W.; Kim, J. K.; Bozuyuk, U.; Dogan, N. O.; Khan, M. T. A.; Shiva, A.; Wild, A. M.; Sitti, M. Multifunctional 3D-printed pollen grain-inspired hydrogel microrobots for on-demand anchoring and cargo delivery. *Adv. Mater.* **2023**, *35*, 2209812.

[14] Khodambashi, R.; Alsaid, Y.; Rico, R.; Marvi, H.; Peet, M. M.; Fisher, R. E.; Berman, S.; He, X. M.; Aukes, D. M. Heterogeneous hydrogel structures with spatiotemporal reconfigurability using addressable and tunable voxels. *Adv. Mater.* **2021**, *33*, 2005906.

[15] Weng, G. S.; Thanneeru, S.; He, J. Dynamic coordination of Eu-iminodiacetate to control fluorochromic response of polymer hydrogels to multistimuli. *Adv. Mater.* **2018**, *30*, 1706526.

[16] Li, Z.; Liu, P. C.; Ji, X. F.; Gong, J. Y.; Hu, Y. B.; Wu, W. J.; Wang, X. N.; Peng, H. Q.; Kwok, R. T. K.; Lam, J. W. Y. et al. Bioinspired simultaneous changes in fluorescence color, brightness, and shape of hydrogels enabled by AIEgens. *Adv. Mater.* **2020**, *32*, 1906493.

[17] Zhang, H.; Koens, L.; Lauga, E.; Mourran, A.; Möller, M. A light-driven microgel rotor. *Small* **2019**, *15*, 1903379.

[18] Paikar, A.; Novichkov, A. I.; Hanopolskyi, A. I.; Smaliak, V. A.; Sui, X. M.; Kampf, N.; Skorb, E. V.; Semenov, S. N. Spatiotemporal regulation of hydrogel actuators by autocatalytic reaction networks. *Adv. Mater.* **2022**, *34*, 2106816.

[19] Bi, Y. H.; Du, X. X.; He, P. P.; Wang, C. Y.; Liu, C.; Guo, W. W. Smart bilayer polyacrylamide/DNA hybrid hydrogel film actuators exhibiting programmable responsive and reversible macroscopic shape deformations. *Small* **2020**, *16*, 1906998.

[20] Xue, P.; Bisoyi, H. K.; Chen, Y. H.; Zeng, H.; Yang, J. J.; Yang, X.; Lv, P. F.; Zhang, X. M.; Priimagi, A.; Wang, L. et al. Near-infrared light-driven shape-morphing of programmable anisotropic hydrogels enabled by MXene nanosheets. *Angew. Chem., Int. Ed.* **2021**, *60*, 3390–3396.

[21] Zhu, Q. L.; Du, C.; Dai, Y. H.; Daab, M.; Matejdes, M.; Breu, J.; Hong, W.; Zheng, Q.; Wu, Z. L. Light-steered locomotion of muscle-like hydrogel by self-coordinated shape change and friction modulation. *Nat. Commun.* **2020**, *11*, 5166.

[22] Ye, S.; Ma, W. J.; Fu, G. D. A novel nature-inspired anisotropic hydrogel with programmable shape deformations. *Chem. Eng. J.* **2022**, *450*, 137908.

[23] Cui, H. L.; Pan, N.; Fan, W. X.; Liu, C. Z.; Li, Y. H.; Xia, Y. Z.; Sui, K. Y. Ultrafast fabrication of gradient nanoporous all-polysaccharide films as strong, superfast, and multiresponsive actuators. *Adv. Funct. Mater.* **2019**, *29*, 1807692.

[24] Gevorkian, A.; Morozova, S. M.; Kheiri, S.; Khuu, N.; Chen, H. Y.; Young, E.; Yan, N.; Kumacheva, E. Actuation of three-dimensional-printed nanocolloidal hydrogel with structural anisotropy. *Adv. Funct. Mater.* **2021**, *31*, 2010743.

[25] Zhou, X. H.; Li, T. Z.; Wang, J. H.; Chen, F.; Zhou, D.; Liu, Q.; Li, B. J.; Cheng, J. Y.; Zhou, X. C.; Zheng, B. Mechanochemical regulated origami with tough hydrogels by ion transfer printing. *ACS Appl. Mater. Interfaces* **2018**, *10*, 9077–9084.

[26] Xu, Z. X.; Fu, J. Programmable and reversible 3D-/4D-shape-morphing hydrogels with precisely defined ion coordination. *ACS Appl. Mater. Interfaces* **2020**, *12*, 26476–26484.

[27] Zhang, Y. C.; Liao, J. X.; Wang, T.; Sun, W. X.; Tong, Z. Polyampholyte hydrogels with pH modulated shape memory and spontaneous actuation. *Adv. Funct. Mater.* **2018**, *28*, 1707245.
[28] Zhao, Z. G.; Zhang, K. J.; Liu, Y. X.; Zhou, J. J.; Liu, M. J. Highly stretchable, shape memory organohydrogels using phase-transition microinclusions. *Adv. Mater.* **2017**, *29*, 1701695.
[29] Qu, G. W.; Huang, J. J.; Li, Z.; Jiang, Y. G.; Liu, Y.; Chen, K.; Xu, Z. Y.; Zhao, Y.; Gu, G. S.; Wu, X. W. et al. 4D-printed bilayer hydrogel with adjustable bending degree for enteroatmospheric fistula closure. *Mater. Today Bio* **2022**, *16*, 100363.
[30] Ma, Y. F.; Hua, M. T.; Wu, S. W.; Du, Y. J.; Pei, X. W.; Zhu, X. Y.; Zhou, F.; He, X. M. Bioinspired high-power-density strong contractile hydrogel by programmable elastic recoil. *Sci. Adv.* **2020**, *6*, eabd2520.
[31] Chen, M. Q.; Cui, Y. D.; Wang, Y. X.; Chang, C. Y. Triple physically cross-linked hydrogel artificial muscles with high-stroke and high-work capacity. *Chem. Eng. J.* **2023**, *453*, 139893.
[32] Zhang, Y. Y.; Fan, G. L.; Jiang, J. Q.; Liu, Z. T.; Liu, Z. W.; Li, G. Light-guided growth of gradient hydrogels with programmable geometries and thermally responsive actuations. *ACS Appl. Mater. Interfaces* **2022**, *14*, 29188–29196.
[33] Wen, X.; Zhang, Y.; Chen, D.; Zhao, Q. Reversible shape-shifting of an ionic strength responsive hydrogel enabled by programmable network anisotropy. *ACS Appl. Mater. Interfaces* **2022**, *14*, 40344–40350.
[34] Lu, Z.; Sun, L. W.; Liu, J. P.; Wei, H. Q.; Zhang, P.; Yu, Y. Photoredox-mediated designing and regulating metal-coordinate hydrogels for programmable soft 3D-printed actuators. *ACS Macro Lett.* **2022**, *11*, 967–974.
[35] Lu, H. H.; Wu, B. Y.; Yang, X. X.; Zhang, J. W.; Jian, Y. K.; Yan, H. Z.; Zhang, D. C.; Xue, Q. J.; Chen, T. Actuating supramolecular shape memorized hydrogel toward programmable shape deformation. *Small* **2020**, *16*, 2005461.
[36] Habault, D.; Zhang, H. J.; Zhao, Y. Light-triggered self-healing and shape-memory polymers. *Chem. Soc. Rev.* **2013**, *42*, 7244–7256.
[37] Obiweluozor, F. O.; GhavamiNejad, A.; Maharjan, B.; Kim, J.; Park, C. H.; Kim, C. S. A mussel inspired self-expandable tubular hydrogel with shape memory under NIR for potential biomedical applications. *J. Mater. Chem. B* **2017**, *5*, 5373–5379.
[38] Davidson-Rozenfeld, G.; Stricker, L.; Simke, J.; Fadeev, M.; Vázquez-González, M.; Ravoo, B. J.; Willner, I. Light-responsive arylazopyrazole-based hydrogels: Their applications as shape-memory materials, self-healing matrices and controlled drug release systems. *Polym. Chem.* **2019**, *10*, 4106–4115.
[39] Liu, W.; Geng, L. H.; Wu, J. M.; Huang, A.; Peng, X. F. Highly strong and sensitive bilayer hydrogel actuators enhanced by cross-oriented nanocellulose networks. *Compos. Sci. Technol.* **2022**, *225*, 109494.
[40] Lu, Y.; Han, J. Q.; Ding, Q. Q.; Yue, Y. Y.; Xia, C. L.; Ge, S. B.; Van Le, Q.; Dou, X. M.; Sonne, C.; Lam, S. S. TEMPO-oxidized cellulose nanofibers/polyacrylamide hybrid hydrogel with intrinsic self-recovery and shape memory properties. *Cellulose* **2021**, *28*, 1469–1488.
[41] Dong, H.; Snyder, J. F.; Williams, K. S.; Andzelm, J. W. Cation-induced hydrogels of cellulose nanofibrils with tunable moduli. *Biomacromolecules* **2013**, *14*, 3338–3345.
[42] Yao, K.; Huang, S.; Tang, H.; Xu, Y. P.; Buntkowsky, G.; Berglund, L. A.; Zhou, Q. Bioinspired interface engineering for moisture resistance in nacre-mimetic cellulose nanofibrils/clay nanocomposites. *ACS Appl. Mater. Interfaces* **2017**, *9*, 20169–20178.